

Experimental Investigation of Laminar Flame Speed Measurement for Kerosene Fuels: Jet A-1, Surrogate Fuel, and Its Pure Components

Yi Wu,^{*,†,‡,§} Vincent Modica,[‡] Xilong Yu,[†] and Frédéric Grisch[‡]

[†]State Key Laboratory of High Temperature Gas Dynamics, Institute of Mechanics, Chinese Academy of Sciences, Beijing 100190, China

[‡]CORIA-UMR 6614, Normandie Université, CNRS, INSA et Université de Rouen, Campus Universitaire du Madrillet, 76800 Saint-Etienne du Rouvray, France

ABSTRACT: The present work investigated the laminar flame speed measurement of kerosene-relevant fuel, including Jet A-1 commercial kerosene, and surrogate kerosene fuel and its pure components (*n*-decane, *n*-propyl benzene, and propyl cyclohexane) using a high-pressure Bunsen flame burner. The OH* chemiluminescence technique and the kerosene-PLIF technique were used for flame contours detection in order to calculate the laminar flame speed. The experiments were first conducted for *n*-decane/air flame at $T = 400$ K, $\phi = 0.6$ –1.3, and atmospheric pressure conditions in order to validate the whole experimental system and measurement methodology. The laminar flame speed of Jet A-1/air, surrogate/air, and pure kerosene component (*n*-decane, *n*-propyl benzene, and propyl cyclohexane) was then measured under large operating conditions, including temperature $T = 400$ –473 K, pressure $P = 0.1$ –1.0 MPa, and equivalence ratio $\phi = 0.7$ –1.3. It was found that these three pure components of kerosene have very similar laminar flame speed. By comparing the experimental results of surrogate kerosene and Jet A-1 commercial kerosene, it was observed that the proposed surrogate kerosene, i.e., mixtures of 76.7 wt % *n*-decane, 13.2 wt % *n*-propyl benzene, and 10.1 wt % propyl cyclohexane, can appropriately reproduce the flame speed property of Jet A-1 commercial kerosene fuel. The experimental results were further compared with simulation results using a skeletal kerosene mechanism.

1. INTRODUCTION

Understanding the fundamental combustion properties of commercial jet fuels is essential in the development of low-cost and efficient aircraft engines. For this purpose, as well as to improve the performance of aeronautical propulsion systems, a comprehensive understanding of the chemical kinetic mechanisms of multicomponent commercial jet fuels is needed.¹ However, the detailed chemical mechanisms of commercial jet fuels, such as Jet A-1, consist of several hundreds of different species and about 1000 elementary reactions. To perform mechanical CFD (computational fluid dynamics) simulations using detailed kinetic mechanisms, we need to get solutions of all transport equations for each species present in the detailed kinetic mechanism and calculate all of the source terms for each species. This kind of simulation of an industrial complex geometry using the aforementioned detailed kinetic mechanism remains elusive.² In practical investigations, an alternative approach is using pure hydrocarbon fuels or composition-simplified surrogate fuels to simulate the physicochemical characteristics of practical kerosene fuels.^{3–8} One of the indicators for validation of surrogate kerosene is the similarity between the combustion properties and those of multicomponent practical fossil fuels.⁹ Therefore, it is first of substantial interest to learn about the surrogate fuel combustion characteristics and associated chemical mechanism in order to more effectively exploit commercial jet fuels. Several methodologies have been used to quantify fundamental properties of surrogate jet fuels, such as ignition,^{10–15} laminar flame speed,^{7,16–22} flame stretch, and extinction limit.^{11,23–27} Among these parameters, laminar flame speed is a key

parameter to understand the reactivity, diffusivity, and exothermicity of fuel/air mixtures and validating both kinetic chemical mechanisms and turbulent models.^{28,29}

The aforementioned necessities have motivated numerous previous works, which have investigated the laminar flame speed of composition-simplified surrogate kerosene fuel and their pure components.^{10,19,30–41} Typically, commercial kerosene, such as Jet A-1, involves around 50–65% paraffin, 10–20% aromatics, and 20–30% naphthenic, which cause the elucidation of the main components of previously proposed surrogate kerosene.⁴² In the early stages of a kerosene surrogate investigation, the composition of the surrogates generally comprised more than 10 kinds of hydrocarbons fuels.^{30,35} Investigations were then performed to reduce the number of compositions to less than 10, because it was commonplace to compose the surrogates in using some compositions in practical fuels, including low-concentration components, such as naphthalene and several hydrocarbons of the same category.³⁶ More recently, the composition of surrogate fuels has continually been simplified to culminate in one-, two-, or three-component surrogate fuels.^{10,30–34} A review of the literature reveals that the Aachen surrogate⁵ and the UCSD surrogate³⁴ can well reproduce the property of autoignition and the extinction rate of commercial kerosene fuels. Laminar flame speed measurements of the Aachen surrogate fuel have been performed with the spherically expanding flame method under

Received: September 13, 2017

Revised: December 27, 2017

Published: January 11, 2018



conditions of $P = 0.1$ MPa and $T = 473$ K. Holley et al.²⁵ conducted measurements of the extinction strain rate and ignition temperature of the surrogate fuels with a counter-flow burner under atmospheric pressure and elevated preheating temperature conditions. In their work, they also compared single-component hydrocarbon with a surrogate jet fuel of JP-8. More recently, Comandini et al.⁷ measured laminar flame speeds of surrogate fuel composed by *n*-decane, *n*-butyl benzene, and *n*-propyl benzene using the spherically expanding flame method under conditions of $T = 403$ K and $P = 0.1$ MPa. Laminar flame speeds of surrogate mixtures were compared with each pure component and discussed in detail.⁷ Besides the aforementioned Aachen surrogate⁵ and the surrogate referred to in the work of Comandini et al.,⁷ few investigations of laminar flame speed measurements for other surrogate fuels can be found in the literature. Comparisons of laminar flame speeds between surrogate fuel and commercial kerosene fuels have been rarely performed. In the present work, surrogate kerosene consisting of *n*-decane (76.7 wt %), *n*-propyl benzene (13.2 wt %), and propyl cyclohexane (10.1 wt %) was investigated for their laminar flame speeds using a high-pressure Bunsen flame burner.^{43,44} This composition of surrogate for kerosene was initially referred to in the work of Dagaut et al.⁸ and Luche et al.,⁶ who developed a skeletal kinetic mechanism targeting to emulate the combustion properties of commercial kerosene fuels. However, to the best of our knowledge, no measurements of laminar flame speeds were performed and compared with commercial kerosene fuels for this three-component surrogate kerosene. In the present work, in order to evaluate the performance of this surrogate fuel, its laminar flame speed will be measured under a large range of conditions, including variations of temperature, pressure, and equivalence ratio, and compared with the laminar flame speed of commercial kerosene fuel (Jet A-1).

In order to compare the flame speed of the surrogate kerosene proposed in the present work with commercial kerosene, laminar flame speed measurements of Jet A-1 kerosene fuel/air mixtures under the same conditions as for the aforementioned surrogate kerosene have been performed. A review of the literature reveals that even though commercial kerosene (such as Jet A-1) fuel has been used for decades in aeronautics, it has only been in recent years that its laminar flame speeds have been measured with reasonable accuracy, owing to the development of the measurement devices used.^{18,19,37–41} For instance, Kumar et al.³⁷ measured laminar flame speeds of Jet A-1 using the counter-flow flame method under atmospheric pressure conditions and temperatures of 400, 450, and 470 K. Hui et al.¹⁹ also measured the laminar flame speed of Jet A-1 using the counter-flow method; in their work efforts were focused on measurements in higher pressure conditions of $P = 0.1–0.3$ MPa, with preheated temperatures between 350 and 470 K and equivalence ratios from 0.7 to 1.3. In their work, the unstretched laminar flame speed was determined by the linear extrapolation of the stretched laminar flame speeds. While both of the measurements^{19,37} were performed using the same counter-flow flame burner, large data deviation was observed. Other laminar flame speed measurements of Jet A-1 were depicted in the investigation of Chong et al.¹⁸ The PIV optical technique has been applied on a jet wall stagnation flame to determine the laminar flame speed of Jet A-1. Regarding the laminar flame speed of Jet A-1 measured under pressure conditions higher than 0.5 MPa, to the best of the authors' knowledge, the only experimental data available are

found in the work of Vukadinovic et al.³⁸ In their study, the laminar flame speeds were measured at a pressure of up to 0.8 MPa using the spherically expanding flame method. Generally, as a summary of the above literature, large data scattering (up to 15 cm/s) is observable between the different results of laminar flame speeds for Jet A-1 fuel.^{19,37,39–41} Even though part of the discrepancies are due to the fact that the composition of Jet A-1 varies among different production regions, further investigation is still necessary to restrain the uncertainties introduced by methodologies, such as linear or nonlinear correlations, and by measurements devices. Moreover, measurements under high-pressure and elevated temperature conditions in the propulsion system are still deficient, such that further investigations into accurate laminar flame speed measurements of kerosene fuels are still necessary.

In the present work, laminar flame speeds of kerosene fuels, including Jet A-1 commercial kerosene, as well as Luche surrogate fuel and its pure components, i.e., *n*-decane, *n*-propyl benzene, and propyl cyclohexane, are measured under large operating conditions, including variations in temperature, pressure, and equivalence ratio based on a high-pressure Bunsen flame burner. The OH* chemiluminescence optical technique and the kerosene-PLIF technique were used for flame contours detection in order to calculate the laminar flame speed. OH* chemiluminescence is a convenient and widely applied combustion diagnostic technique; however, for Bunsen flames with large molecular weight fuels, flame tip opening phenomenon occurs under slight fuel-rich conditions (around $\varphi > 1.15–1.2$). Under these conditions, OH* chemiluminescence has difficulty in obtaining the whole flame contours due to local quenching at the cusp of the flame.^{45–48} Kerosene-PLIF has the advantage of visualizing the contours of the unburned fronts of kerosene/mixtures, such as Jet A-1, which is free from the influence of local quenching located in the burned gas.^{49,50} Hence, in the present work, kerosene-PLIF is applied to validate the suitable flame contours definition for the OH* chemiluminescence technique when the flame-opening phenomenon conditions are present.

Experimental results of *n*-decane/air mixtures using the OH* chemiluminescence technique will first be presented to validate the accuracy of the whole experimental system and the determination methodology. For further investigating the effect of the flame-opening phenomenon on the laminar flame speed measured by OH* chemiluminescence, comparison of the laminar flame speeds obtained by OH* chemiluminescence and the kerosene-PLIF technique for Jet A-1/air mixtures under the same operating conditions are performed. Measurements are then extended to higher temperatures $T = 400, 423,$ and 473 K for pure surrogate components, i.e., *n*-decane, *n*-propyl benzene, and propyl cyclohexane under atmospheric pressure conditions. Finally, the laminar flame speed of surrogate kerosene, i.e., mixtures of *n*-decane (76.7 wt %), *n*-propyl benzene (13.20 wt %), and propyl cyclohexane (10.1 wt %), are measured under conditions of $T = 400–473$ K, $P = 0.1–1.0$ MPa, and $\varphi = 0.7–1.3$ and then compared with the experimental results of commercial kerosene (Jet A-1) measured under identical conditions. The laminar flame speed of surrogate fuel is also simulated with a skeletal kerosene mechanism. Further analysis and discussions will be detailed.

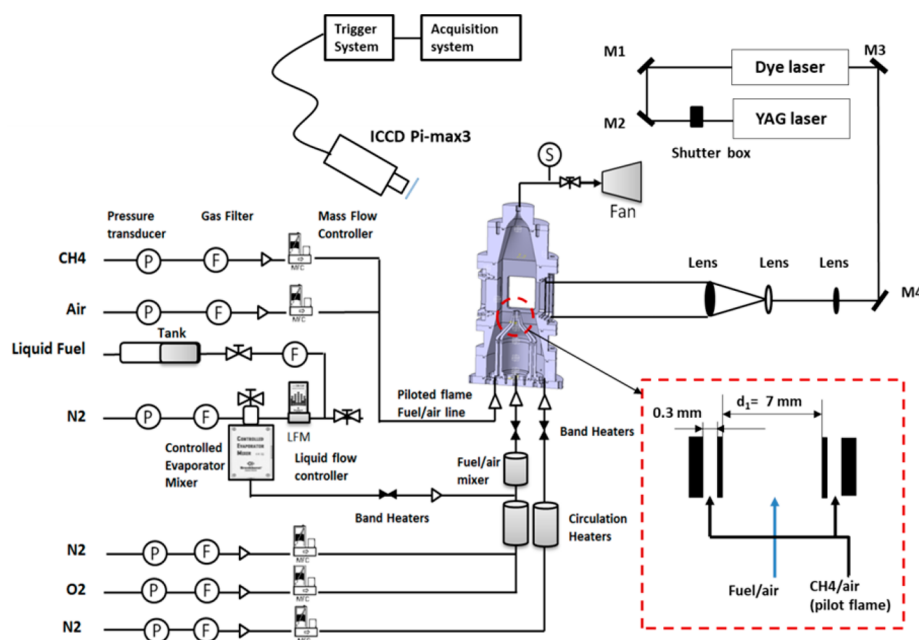


Figure 1. Schematic of the experimental setup.

2. EXPERIMENTAL METHODOLOGY

2.1. High-Pressure Burner and Gas Feeds. In the present study, a high-pressure Bunsen flame burner was developed to measure the laminar flame speed of kerosene fuels. The detailed description of the experimental apparatus can be found in Wu et al.'s previously published work;^{43,44} as such, only a brief introduction is given here.

As illustrated in Figure 1, the whole experimental apparatus consists of a high-pressure Bunsen flame burner, liquid fuel vaporization with a gas feed system, and an optical diagnostic setup. With this system, a steady conical flame can be generated on the outlet of the contoured nozzle that has an outlet diameter of 7 mm. A concentric contoured nozzle with an outlet diameter of $d_2 = 7.6$ mm, which surrounds the central nozzle, is used to produce a pilot flame in order to stabilize the flame under high-pressure operating conditions. The equivalence ratio and the flow rate of the pilot flame are regulated by two mass flow controllers. The whole burner is placed in an N_2 (guard flow) ventilated high-pressure chamber. A liquid flow controller (Bronkhorst mini-CORIFLOW) is used to deliver liquid kerosene fuel to the controlled evaporator and mixer (CEM, Bronkhorst), where the liquid fuel and N_2 carrier gas are mixed and heated to a preset temperature. The CEM system allows one to vaporize liquid kerosene fuel, and two additional flow controllers were used to deliver nitrogen and oxygen to mix at the outlet of CEM to reproduce the synthetic species' composition of air and control the equivalence ratio of vaporized fuel/air mixtures. The whole chamber and all gas feed lines are preheated with electrical wire heaters. Five thermocouples located in different positions of the high-pressure chamber are used to measure and monitor the uniformity of the temperature throughout the pressure chamber. The pressure in the chamber is measured with a piezoelectric transducer located at the outlet of the high-pressure chamber. Two circulation heaters are used to heat the guard flow and the vaporized fuel/air mixture to avoid condensations of the fuel vapor. There are four UV quartz windows at the high-pressure chamber, allowing probing the flame with optical diagnostics.

2.2. Optical Diagnostic Setup. 2.2.1. OH^* Chemiluminescence.

One of the optical techniques used in the present work to detect the flame contour is the OH^* chemiluminescence imaging technique. A thermoelectrically cooled, 16-bit intensified CCD camera (PI-MAX 3, Roper Scientific) was used to record the OH^* chemiluminescence flame image. With an achromatic UV lens (CERCO) of $f/2.8$, $f = 100$ mm, and an interference band-pass filter centered at 310 nm, the camera can visualize a 40×40 mm² area of the flame with a $1024 \times$

1024 array so that the spatial resolution is about $40 \mu\text{m}$ per pixel. The exposure time to record the OH^* chemiluminescence image is controlled by opening the intensifier gate $1 \mu\text{s}$. The acquisition repetition rate of the camera is set to 10 Hz.

2.2.2. Kerosene-PLIF. It is well known that the composition of kerosene commonly used in civil engines (i.e., Jet A1) consists of a wide range of hydrocarbon molecules. Among these, aromatic molecules are known to have UV and visible transitions exhibiting strong fluorescence. Therefore, kerosene fuel benefits from its broad-band fluorescence emission between the 260 and 420 nm spectral domains.^{49,50} This fluorescence emission that results from the excitation of aromatics (i.e., mono- and diaromatics) allows visualizing the fresh gas region of the flame. Although aromatics may be excited on a wide range of wavelengths, for a flame to visualize only the unburned gas, the excitation wavelength of kerosene must be selected carefully to avoid overlaps with the resonance of an OH radical transition located in the burned gas. An observation of the fluorescence spectrum of the OH transition reveals that the Q1(5) and Q1(6) rotational lines are well separated, thus presenting the possibility to tune the excitation wavelength of aromatics to 282.85 nm in a spectral region in which only the aromatics fluorescence will be collected.

In the present work, the kerosene planar laser-induced fluorescence system consists of a cluster system, which includes a Nd:YAG laser (Quanta-ray Pro-190), a dye laser (Sirah PRSC-G-300), and a high-resolution ICCD camera (PI-MAX 3, Roper Scientific). A frequency-doubled, Q-switched Nd:YAG laser was used to pump a dye laser, which was then frequency doubled to obtain wavelengths in the 280–290 nm spectral range. The dye laser was tuned to 282.85 nm to excite the aromatics in the Jet A-1 fuel. The laser energy was regulated to 5 mJ in order to keep the fluorescence of kerosene within the linear regime, thus maintaining the proportionality between the intensity of fluorescence and the concentration of kerosene fuel. The UV laser beam at the exit of the laser source was transported via optical mirrors. It was then transformed into one 50 mm collimated sheet using a set of converging and divergent cylindrical lenses and a spherical lens. The two cylindrical lenses formed a telescope, which sped up the beam into a collimated sheet to cross the target flame. The kerosene fluorescence image was then recorded by the ICCD camera (the same one used for the OH^* chemiluminescence technique). The intensifier gate width was set to $1 \mu\text{s}$, and the framing rate of the acquisition of fluorescence images was 10 Hz. The camera was equipped with the same optical lens with OH^* chemiluminescence, while only the optical filter was

changed to 300–550 nm. As shown in Figure 2, images of Jet A-1/air flames using the OH* chemiluminescence technique and the kerosene-PLIF technique are presented.

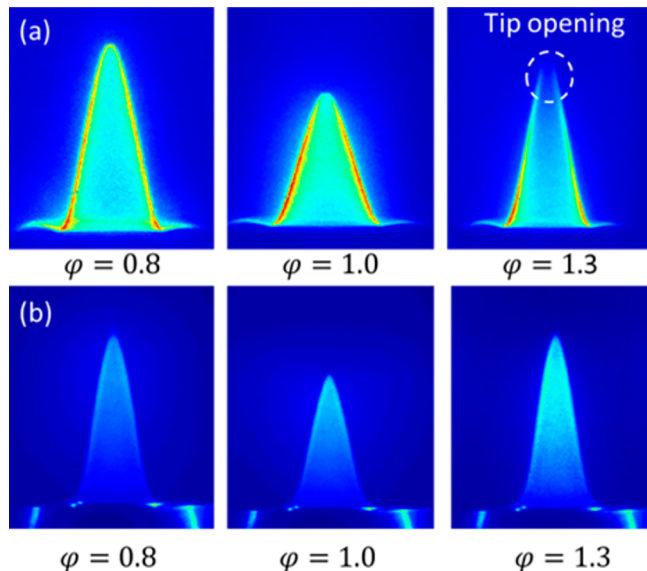


Figure 2. Jet A-1/air flames under the conditions of $T = 400$ K, $P = 0.1$ MPa for equivalence ratios $\phi = 0.8$, 1.0, and 1.3: (a) OH* chemiluminescence technique; (b) Kerosene-PLIF technique.

2.3. Fuel Properties. The chemicals used in the different mixtures were *n*-decane ($C_{10}H_{22}$, Sigma-Aldrich, 99+%), *n*-propyl benzene (C_9H_{12} , Aldrich, 99+%), and *n*-propyl cyclohexane (C_9H_{18} , Aldrich, 99+%). The Luche surrogate fuel for emulating the commercial jet fuel is a mixture of these three components by *n*-decane (76.7 wt %), *n*-propyl benzene (13.2 wt %), and propyl cyclohexane (10.1 wt %). The average chemical formula is $C_{9.74}H_{20.05}$ with a molar mass equal to 136.93 g/mol. Meanwhile, the target commercial kerosene fuel used in the present work was analyzed by gas chromatography, and its chemical composition is shown in Table 1. The chemical composition

Table 1. Chemical Composition of Jet A-1 in the Present Study

species	proportion (wt %)
paraffin	46.5
noncondensed naphthene	22.3
condensed naphthene	13.2
alkylbenzenes	13.2
indanes and tetralines	2.8
naphthalenes	1.8
acenaphthenes and diphenyls	0.1
benzothiophenes	0.1
saturated	82
monoaromatic	16
diaromatic	1.9
sulfur	0.1

of this fuel consists mainly of paraffin, naphthenic, and alkyl benzenes. In addition, there is no hydrocarbon polyaromatic hydrocarbon heavier than naphthalene. The average chemical formulation of Jet A-1 is $C_{11.16}H_{20.82}$ with a molar mass equal to 154 g/mol. Table 2 summarizes the properties of studied fuels in the present work.

2.4. Extraction of Flame Speed. The Bunsen flame method is a convenient and widely used approach for laminar flame speed measurements because of its advantages of simplicity and a well-defined flame structure. Laminar flame speed is defined as the velocity

Table 2. Fuel Property of *n*-Decane, *n*-Propylene, Propyl Cyclohexane, Luche Surrogate, and Jet A-1 Fuel

fuel	formula	boiling point (K)	density (kg/m^3)
<i>n</i> -decane	$C_{10}H_{22}$	447.3	724.0
<i>n</i> -propyl benzene	C_9H_{12}	432.4	825.7
propyl cyclohexane	C_9H_{18}	429.9	793.0
Luche surrogate	$C_{9.74}H_{20.05}$	432–447	747.0
Jet A-1	$C_{11.16}H_{20.82}$	423–533	815.9

at which a planar flame front travels relative to the unburned gas in the direction of the flame surface.⁵¹ For a conical flame, with the hypothesis that the flame speed is identical all over the entire surface area of the flame, the laminar flame speed can be calculated, based on the mass conservation between the outlet nozzle and the flame

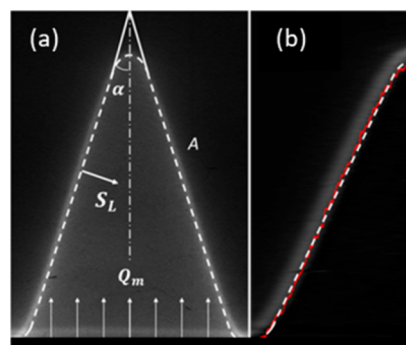


Figure 3. Determination of the flame surface area: (a) initial OH* chemiluminescence image and (b) left part of the Abel-inverted image (red line is the initial flame contours determined by taking the inside front of the Abel-inverted image, while dashed line is the flame contours used in flame speed calculations made following the smoothing function).

front.^{44,52–56} As shown in Figure 3, the average flame speed in the transverse plane is expressed by

$$\rho_u S_L A = Q_m \rightarrow S_L = Q_m / (\rho_u A) \quad (1)$$

where Q_m is the total mass flow rate of the fuel/air gaseous mixture and ρ_u is the density of fresh gas. This method requires the knowledge of the total area of the flame surface A , which is determined in the present investigation by analyzing the OH* chemiluminescence image and the kerosene-PLIF image (for Jet A-1 fuel) of the flames. Kerosene-PLIF is applied to validate the OH* chemiluminescence image-processing algorithm for the cases when the flame tip-opening phenomenon is present. For large molecule weight fuel, such as kerosene, the flame tip-opening phenomenon appears when the equivalence ratio is higher than around $\phi > 1.15$ –1.2. The tip opening of the laminar Bunsen flame involves local combustion extinction, which occurs at the top part of the flame where a strong negative flame stretch presents.^{45,46} When the OH* chemiluminescence technique is applied, as illustrated in Figure 2 (for the case $\phi = 1.3$), the tip-opening phenomenon greatly increases the uncertainties of flame contours determination of the top part of the flame. Fortunately, Kerosene-PLIF, as applied in the current work, has the advantage of directly imaging the unburned fuel/air mixture contour, which is free from the influence of the tip-opening phenomenon. The image-processing procedures are detailed in the following sections.

2.4.1. OH* Chemiluminescence. In order to obtain the two-dimensional flame front of the reaction zone of the OH* chemiluminescence, the recorded image is transformed by Abel inversion using a MATLAB program.⁵⁷ By taking the inside flame front of the image after Abel inversion, the surface A can be calculated. The inside boundary is used because its laminar flame speed is defined by the velocity relative to the unburned premixed gas in the direction

of the flame surface. As the inside boundary is more attracted to fresh gas, it is more appropriate to use it as the flame boundary in order to calculate flame speed.

A specific high-frequency filtering function was used to smooth the resulting curve plotted along the red line in Figure 3 and obtain the final flame front. For equivalence ratio fuel-lean conditions when the flame tip-opening phenomenon has not occurred, the flame contours can be accurately detected using the above-described image-processing method. However, for cases where the flame-opening phenomenon is present, due to the local quenching of the OH* signal, the flame contours are difficult to detect at the flame tip part. In such cases, the flame area that is used for flame speed determination is obtained by extending the linear peripheral contour to the tip of the flame with the application of a high-order interpolation method, as illustrated in Figure 3. The accuracy of the OH* chemiluminescence image-processing method will be further evaluated by the kerosene-PLIF technique.

After obtaining the flame contours, flame area A can be calculated by the pivoting flame front profile $f(x)$ along the burner axis using the following equation

$$A = 2\pi \int_a^b f(x) \sqrt{1 + |f'(x)|^2} dx \quad (2)$$

where a and b are the boundary limits of the flame contours and $f(x)$ is the flame contour profile function obtained by image processing. Assuming the axisymmetric condition of the flame, the final flame speed is the averaged value of the flame surface area, obtained from each half of the recorded images. It should be noted that the flame speed measured using the aforementioned equation is an averaged value of the entire flame surface, which is different from the unstretched flame speed, as this conical flame is affected by its strain and curvature effects. To avoid the effect of the flame, the stretch, and the flame tip-opening phenomenon, for each case, the measured flame was controlled in relation to the maximum height allowed by the current experimental configuration in order to alleviate the tip of the flame. Fortunately, the difference between both values was found to be tiny and negligible, which is consistent with the results in refs 44, 52, and 56.

2.4.2. Kerosene-PLIF. Compared to the processing procedures of OH* chemiluminescence imaging, the data processing of kerosene-PLIF is largely simplified. The outer edge of the fresh gases is defined as the position at which the fluorescence of the aromatics molecules disappears (Figure 4). This location corresponds to the frontier

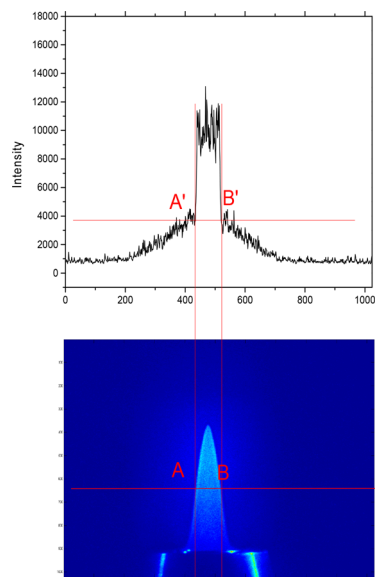


Figure 4. Illustration of the image processing of kerosene-PLIF techniques.

delimiting a chemical transformation of these organic molecules through the action of chemical reactions. Typically, these organic molecules disappear before the OH radical starts to be optically detected. Once the flame front is obtained, the laminar flame speed is determined using the same calculation (eq 2) as the OH* chemiluminescence technique.

2.5. Measurement Uncertainties. For all of the experimental results presented in this work, 30 single-shot images are systematically recorded and the resulting laminar flame speed is determined by the data processing of averaged images, as determined from the set of single-shot images. The measurement uncertainties are mainly associated with the gas/liquid flow delivery system (U_{Qm}) and the uncertainty of the calculated flame area image (U_{Qm}), as determined by the camera resolution. The uncertainty of the total flow rate comes from the mass flow controller uncertainty (0.5% of reading + 0.1% full scale), which is estimated to be $\sim 2\%$, while uncertainty derives from the camera's spatial resolution, which is estimated to be $\sim 3\%$. The overall uncertainty is calculated to be within $\sim 4\%$ (from the relation $U_{Qm}^2 + U_A^2$) for all of the laminar flame speeds recorded under atmospheric pressure conditions. For high-pressure measurements $P > 0.5$ MPa, the measurement uncertainty can be amplified due to flame stability. Indeed, the fluctuation of the position of the flame displays an artificial thickening of the flame front during the time integration of the signal on the camera. This effect modifies the position of the flame contours (2–3 pixels), giving a maximum uncertainty of $\sim 7\%$ in the worst situation.

3. EXPERIMENTAL RESULTS AND DISCUSSION

Experimental results of *n*-decane/air mixtures using the OH* chemiluminescence technique will first be presented in order to validate the accuracy of the aforementioned image-processing methodology and the whole experimental system. To further investigate the effect of the flame-opening phenomenon on the laminar flame speed measured by OH* chemiluminescence, a comparison of the laminar flame speeds obtained by OH* chemiluminescence and the kerosene-PLIF technique for Jet A-1/air mixtures under the same operating conditions is performed. The laminar flame speed of pure surrogate components (*n*-propyl benzene and propyl cyclohexane) is then measured under atmospheric pressure conditions at different temperatures, that is, 400, 423, and 473 K. The laminar flame speed of the kerosene surrogate (mixtures of *n*-decane, *n*-propyl benzene, and propyl cyclohexane) and the Jet A-1/air mixture are then subsequently measured at $T = 400$, 423, and 473 K. High-pressure measurements from 0.1 to 1.0 MPa are performed with an equivalence ratio ranging from 0.7 to 0.8. For high-pressure measurements, the preheated temperature is fixed at $T = 423$ K, with only the equivalence ratio for the fuel-lean side performed. These temperature and equivalence ratio conditions are selected in order to ensure a stabilization of the flame at the nozzle outlet during the experiments and to prevent fuel pyrolysis for temperatures higher than 423 K, especially under elevated pressure conditions. This is essential to guarantee measurement accuracy and make sure that no chemical reaction modifies the fuel composition during the transport of the fuel/air mixture inside the combustion chamber. Experiments are then compared with data found in the literature and the simulation results using the Luche skeletal kerosene mechanism.⁶

3.1. OH* Chemiluminescence Methodology Validation. Preliminary measurements using OH* chemiluminescence are performed for *n*-decane/air mixtures under condition $\varphi = 0.7$ –1.3, $iT = 400$ K, and atmospheric pressure conditions to validate the whole experimental setup and measurement methodology. Laminar flame speeds calculated in the present

work are compared with the literature found experimental results. A review of the literature reveals that *n*-decane is one of the main components in kerosene fuels, while its laminar flame speed has been extensively explored. Figure 5 illustrates the

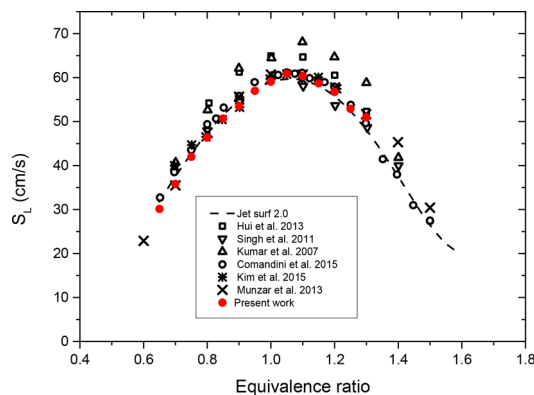


Figure 5. Comparison between our experimental results and the data from the literature of *n*-decane/air mixtures: $\varphi = 0.6$ –1.5, $T = 400$ K, and $P = 0.1$ MPa.

comparison between the experimental results in the present work and the experimental data found from the literature. The simulated flame speeds using the detailed kinetic mechanism JetSurF 2.0 are plotted at the same figure as well. JetSurF 2.0 is a detailed mechanism for kerosene fuels, which consists of 348 species and 2162 reactions, as established by Wang et al.⁵⁸ Except for the results presented by Hui et al.¹⁹ and those reported by Kumar et al.,³⁷ which shows a significant difference from the other measurements, there is a general agreement between our laminar flame speeds and those in the literature, albeit with a better agreement between our data and the JetSurF 2.0 simulation results. Our experimental results show good agreement with the laminar flame speed measured using spherical flames as well.^{7,59,60} However, a tiny difference between our experimental results and the numerical predictions is observed at equivalence ratio $\varphi = 1.3$.

Figure 6 shows experimental results for higher temperature conditions of $T = 423$ and 473 K. As expected, the laminar flame speed increased with the preheating temperature of the mixture. The conditions where the flame tip-opening phenomenon was present are also labeled in the figure. In order to further clarify the influence of the flame tip-opening

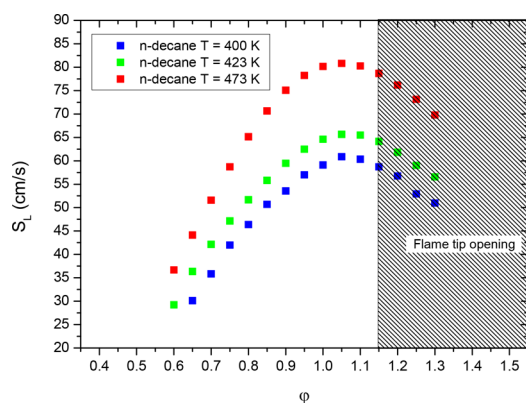


Figure 6. Laminar flame speed of *n*-decane/air mixture at $T = 400$, 423 , and 473 K, $P = 0.1$ MPa, and $\varphi = 0.65$ –1.3.

phenomenon on the determination of the flame speed using the OH* chemiluminescence method, experiments are performed with both the kerosene-PLIF and the OH* chemiluminescence techniques for Jet A-1/air mixtures at $T = 400$ K, $P = 0.1$ MPa, and $\varphi = 0.6$ –1.3. As depicted in Figure 7, laminar flame speeds

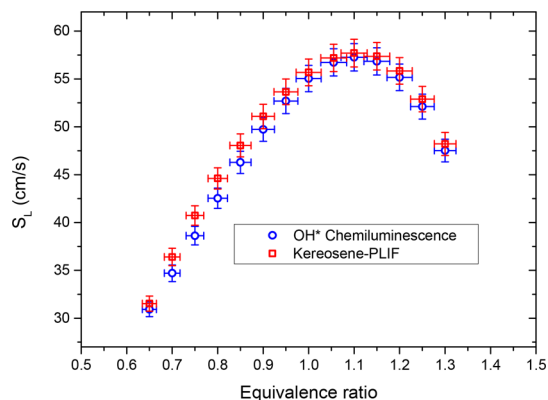


Figure 7. Comparison between laminar flame speeds determined from OH* chemiluminescence and Kerosene-PLIF of Jet A-1/air mixture: $T = 400$ K, $P = 0.1$ MPa, and $\varphi = 0.65$ –1.3.

derived from the kerosene-PLIF technique show general agreement with those determined with OH* chemiluminescence, with a maximum difference of 3 cm/s on the fuel-lean side. There is a better agreement between the results of the OH* chemiluminescence technique and the kerosene-PLIF technique under approaching stoichiometric conditions. For the fuel-rich side, where the flame tip-opening phenomenon is present, the difference between these two techniques is less than 2 cm/s. This illustrates that the OH* chemiluminescence image-processing method proposed in the present work is able to determine the flame speeds with reasonable accuracy when the flame tip-opening phenomenon is present. The experimental results presented in the following sections were obtained using the OH* chemiluminescence technique considering the simplicity of this methodology.

3.2. Laminar Flame Speed of Neat Surrogate

3.2.1. *n*-Propyl Benzene.

n-Propyl benzene is a large molecular weight fuel that can be largely found in kerosene fuels. However, its laminar flame speed has not been widely studied. The only literature results that can be found is the measurements recently performed with the stagnation flame¹¹ and the heat flux methods.⁶¹ Figure 8 plots the experimental results obtained in the present work and those presented in refs 11 and 61. It shows that our experimental results are in accordance with those reported in the work of Mehl et al.⁶¹ for all equivalence ratio conditions investigated. The maximal difference observed from this comparison is around 5 cm/s, which is a value that remains comparable with our measurement uncertainty. Meanwhile, our experimental results show lower flame speeds compared with the results obtained by Hui et al.¹¹ As shown in Figure 9, in order to investigate the effect of preheating temperature on laminar flame speeds, experiments were performed with higher temperatures $T = 423$ and 473 K. As expected, the experimental results show that the laminar flame speed increases with higher temperature conditions.

3.2.2. Propyl Cyclohexane. Propyl cyclohexane is one of the main cycloalkanes that are usually present in kerosene fuels. Different from *n*-alkanes, branched alkanes, or aromatics,

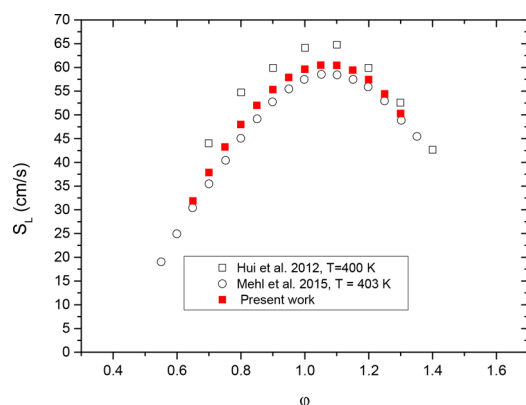


Figure 8. Laminar flame speed of *n*-propyl benzene at $T = 400$ K, $\phi = 0.6$ – 1.3 , and $P = 0.1$ MPa.^{11,61}

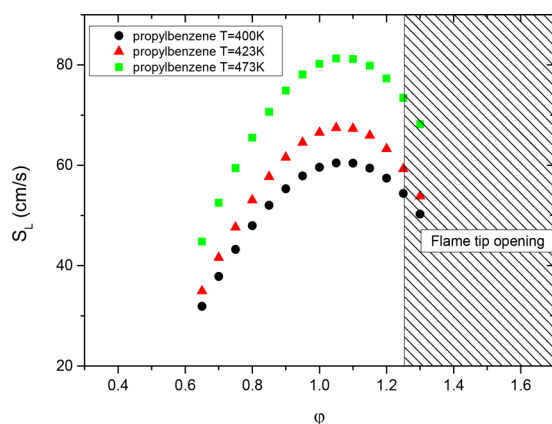


Figure 9. Laminar flame speed of *n*-propyl benzene at $T = 400$ K, 423 and 473 K, $\phi = 0.6$ – 1.3 , and $P = 0.1$ MPa.

laminar flame speed measurements of propyl cyclohexane over a large range conditions of preheating temperature and equivalence can be rarely found in the literature. In the present work, experimental measurements were first performed at $T = 400$ K, $P = 0.1$ MPa, and $\phi = 0.65$ – 1.3 and then compared with the data found in the literature. As shown in Figure 10, at the equivalence ratio on the lean side our experimental results are in accordance both with the results presented in the work of Comandini et al.⁷ (nonlinear extrapolation at a zero stretch rate) and with the results presented in the work of Dubois et al.⁶² (linear extrapolation at a zero stretch rate). However,

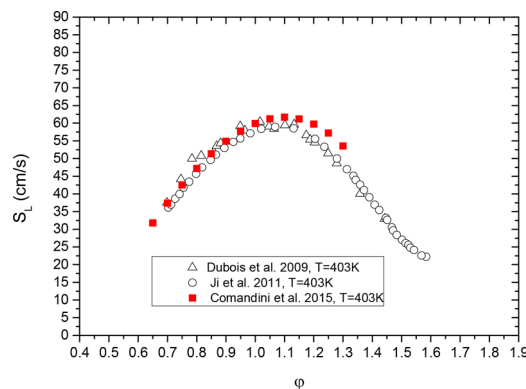


Figure 10. Laminar flame speed of propyl cyclohexane at $T = 400$ K, $P = 0.1$ MPa, $\phi = 0.65$ – 1.3 .^{7,62}

discrepancy was observed that at the fuel-rich side our experimental results give higher laminar flame speed compared with the literature found results. This discrepancy could come from the influence of the tip-opening phenomenon when active for these operating conditions of $\phi = 1.15$ – 1.3 . Experiments were also performed for higher temperature conditions of $T = 423$ and 473 K, as plotted in Figure 11.

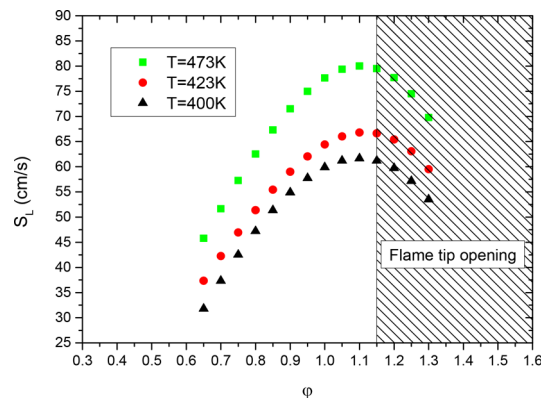


Figure 11. Laminar flame speed of propyl cyclohexane/air mixture at $T = 400$, 423, and 473 K, $P = 0.1$ MPa, and $\phi = 0.65$ – 1.3 .

3.2.3. Comparison between the Pure Components. Figure 12 plots the laminar flame speeds of the three component in

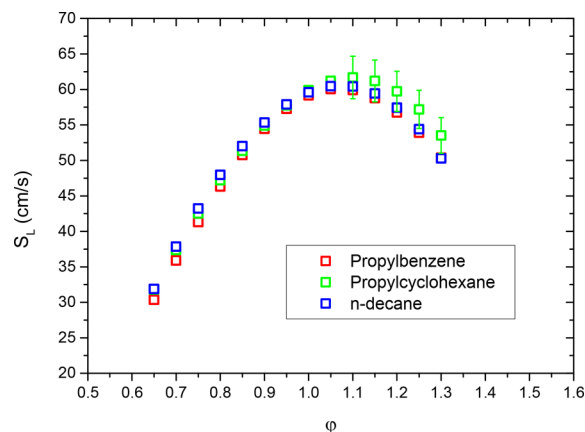


Figure 12. Laminar flame speeds of *n*-decane, *n*-propyl benzene, and *n*-propyl cyclohexane at $T = 400$ K, $P = 0.1$ MPa, and $\phi = 0.65$ – 1.3 .

Luche surrogate fuel at conditions of $T = 400$ K, $P = 0.1$ MPa, and $\phi = 0.65$ – 1.3 . It shows that for all equivalence ratio conditions investigated in the present work the three pure components have quite similar laminar flame speed values. However, a more careful observation of the results reveals that *n*-decane has slightly higher flame speed values (about a maximum of 2.5 cm/s at fuel lean side) than *n*-propyl benzene. This tiny difference can be explained by the different molecular structure between *n*-decane and *n*-propyl benzene. As discussed in the work of Comandini et al.,⁷ *n*-propyl benzene is an aromatic molecule that has a ring chemical structure which potentially has an influence on the combustion reaction. Indeed, a sensitivity analysis explained that the flame speed is affected by the ring structure, in particular, by the reactions involving radical intermediates, such as phenoxy, benzyl, and the phenyl radicals. Moreover, the work of Mehl et al.⁶¹ also

mentioned that the increase of benzyl radicals in the preheating zone restrains flame propagation and can decrease flame speed. The above analysis indicates that the laminar flame speed of propyl cyclohexane is higher than that of *n*-propyl benzene.

As *n*-decane and propyl cyclohexane both belong to the alkane category, they can be directly compared. Our experimental results show that laminar flame speed of *n*-decane (*n*-alkane) is almost identical but uniformly higher than those of propyl cyclohexane (monoalkylated cyclohexane). This observation is in agreement with the work of Ji et al.⁶³ and Wu et al.⁶⁴ In their study it was shown that even though the laminar flame speed of *n*-decane is influenced by the small intermediates, decomposition of the linear structure of *n*-alkane (such as *n*-decane) is faster than decomposition of the ring structure existing in monoalkylated cyclohexane (such as propyl cyclohexane). Therefore, these experimental results shed light on the fact that laminar flame speeds are influenced by both the small intermediates involved in the combustion reactions and the initial step in the fuel decomposition.⁷ For lean equivalence ratio conditions, the above-mentioned tendency is well observed in Figure 12: *n*-decane > propyl cyclohexane > *n*-propyl benzene. However, discrepancies among these measurements are limited (about 2–3 cm/s), meaning that it is difficult to estimate this tendency with accuracy. According to our measurement results, the laminar flame speed of these three components is basically the same at fuel-lean conditions. For fuel-rich mixtures, the propyl cyclohexane obviously shows higher laminar flame speeds than those observed for *n*-decane, which contradicts the results found in the literature. These discrepancies could be caused by the aforementioned flame tip-opening phenomenon, which makes the flame contour determination more difficult. Consequently, the measurement uncertainties increase, making elucidation of the evolution of the different laminar flame speeds more complex. For greater clarity, error bars of the propyl cyclohexane measurements in fuel-rich conditions have been added in Figure 12, representing a global uncertainty of around 4.5%.

3.3. Laminar Flame Speed of Surrogate Kerosene. In this part, laminar flame speeds of the Luche surrogate fuel consisting of *n*-decane (76.7 wt %), *n*-propyl benzene (13.2 wt %), and propyl cyclohexane (10.1 wt %) are investigated in a large range of working conditions, including variation of temperature (400–473 K), pressure (0.1–1.0 MPa), and equivalence ratio ($\phi = 0.6$ –1.3). The measurements are compared with simulation results using the Luche kinetic mechanism and compared to experimental results of neat component of surrogate Luche. Experimental data of Luche surrogate is first plotted with neat component of surrogate in Figure 13. It depicts that the difference between the laminar flame speed of Luche surrogate and its three components is tiny; meanwhile, its laminar flame speed is more approaching *n*-decane. Simulation results of Luche surrogate at $T = 400$ –473 K, $P = 0.1$ MPa, and $\phi = 0.6$ –1.3 conditions are compared and plotted in Figure 14, which shows that the model developed by Luche is effective at predicting laminar flame speeds. For all equivalence ratios investigated, simulation results using the Luche mechanism give slightly lower values compared with experimental results. Meanwhile, it should be noted that this difference is quite close to measurement uncertainties. A comparison of the different temperature conditions also illustrated that the Luche kinetic mechanism effectively predicts that the effect of preheating temperature on laminar flame speed is that higher temperature increases the laminar flame

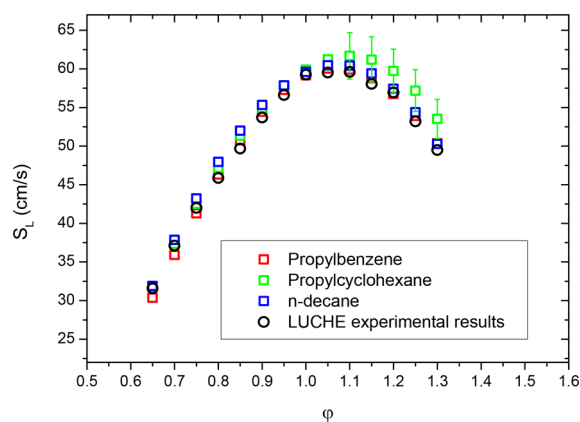


Figure 13. Laminar flame speeds of *n*-decane, *n*-propyl benzene, propyl cyclohexane, and the LUCHE surrogate at conditions of $T = 400$ K, $P = 0.1$ MPa, and $\phi = 0.65$ –1.3.

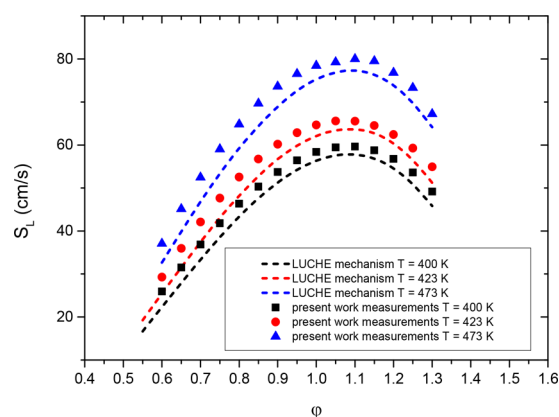


Figure 14. Comparisons between experimental results and simulation results of Luche surrogate fuel with temperature variations ($T = 400$, 423, 473 K, $P = 0.1$ MPa, and $\phi = 0.6$ –1.3).

speed. However, the mechanism underestimates the flame speed of the Luche surrogate about 2–3 cm/s, compared with our measurements for all temperature conditions investigated.

In order to evaluate the capability of the Luche kinetic mechanism under high-pressure conditions, laminar flame speed measurements of Luche surrogate fuel are performed at $T = 423$ K, $\phi = 0.7$ and 0.8, and under pressure conditions from 0.1 to 0.8 MPa. In Figure 15, experimental results of Luche surrogate fuel under high-pressure conditions are compared with simulation results using the Luche skeletal mechanism in a logarithmic graphic. The same as observed at atmospheric pressure conditions, the Luche mechanism gives lower flame speed values compared with our measurements for both equivalence ratios. Meanwhile, the Luche mechanism can well reproduce the effect of pressure on laminar flame speed that the higher pressure gives lower flame speed values for condition of at $\phi = 0.8$, while a discrepancy in the dependence of pressure is observed for conditions of equivalence ratio $\phi = 0.7$. With the increments of pressure, the discrepancy between experiments and simulations tends to increase. However, aforementioned discrepancy must be put into perspective because the maximum difference between the simulation and the experimental results does not exceed 5 cm/s, which is a value comparable to the uncertainty of our measurements under high-pressure conditions. This indicates that the Luche skeletal mechanism

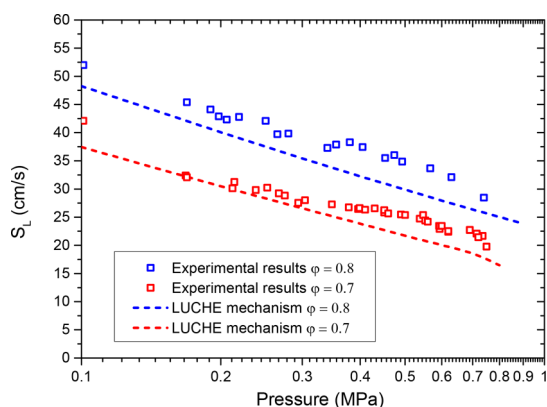


Figure 15. Comparison of laminar flame speeds of the Luche surrogate between experimental results and simulation results at conditions of $T = 423$ K, $\varphi = 0.7$ and 0.8 , and $P = 0.1$ – 0.8 MPa.

performs better under higher rather than lower pressure conditions.

3.4. Laminar Flame Speed of Jet A-1. In this part, laminar flame speed measurements of commercial kerosene fuel Jet A-1 are conducted over a large range of working conditions. Measurements are also performed at high temperature and elevated pressure to investigate temperature and pressure dependency on the laminar flame speed of kerosene Jet A-1. An empirical correlation of the laminar flame speed in taking account of temperature and pressure dependency is then proposed.

As illustrated in Figure 16, the general tendency of the effect of the preheating temperature on the laminar flame speed is in

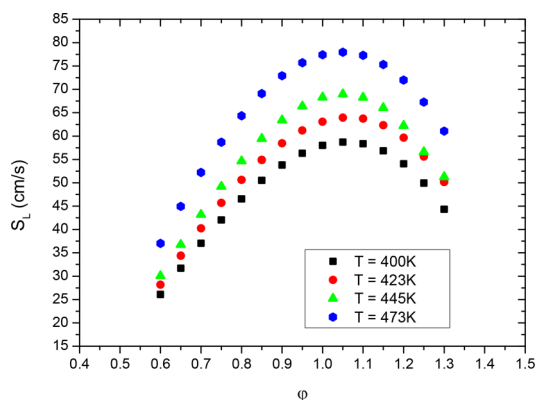


Figure 16. Laminar flame speed of Jet A-1/air with temperature variation: $T = 400$, 423 , 445 , and 473 K, $\varphi = 0.6$ – 1.3 , and $P = 0.1$ MPa.

agreement with theoretical predictions, i.e., the laminar flame speed increases in line with the preheating temperature. According to the power law correlation theory of temperature dependency $S_L = S_{L0} \left(\frac{T}{T_0} \right)^\alpha$,⁴⁴ the laminar flame speed under

higher temperature conditions can be expressed by a laminar flame speed at the reference condition of temperature and pressure (S_{L0}) and multiplied by correction factors displaying the temperature and pressure dependencies. As shown in Figure 17, laminar flame speeds are plotted as a function of the preheating temperature using log–log scales, while straight lines for all of the equivalence ratios tested are observed.

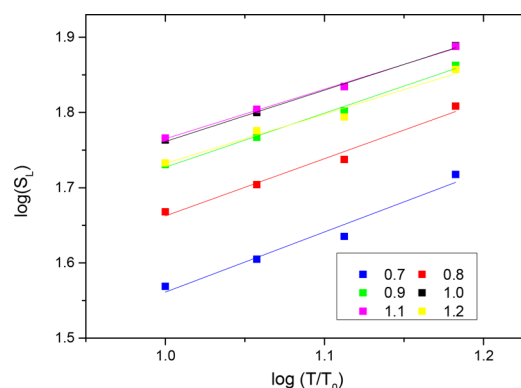


Figure 17. log–log plot of the laminar flame speed of Jet A-1/air under atmospheric pressure and different preheating temperatures (symbols are the experiments, and lines are linear fits).

With the experimental results obtained in the present work, an empirical temperature dependency correlation was proposed by using the power law equation $S_L = S_{L0} \left(\frac{T}{T_0} \right)^\alpha$, where S_{L0} is defined as the laminar flame speed at $T = 400$ K and $P = 0.1$ MPa. The effect of the equivalence ratio is then taken into account by using the extended formulation proposed by Metghalchi and Keck⁶⁵

$$S_{L0}(\varphi) = S_{L0,\varphi=1} + S_{L0,1}(\varphi - 1) + S_{L,2}(\varphi - 1)^2 + S_{L,3}(\varphi - 1)^3 \quad (3)$$

The resulting parameters of α for different equivalence ratios are listed in Table 3.

Table 3. Correlation Parameters $S_{L0,i}$ and α_i

$S_{L0,\varphi=1}$	58.00
$S_{L0,1}$	24.08
$S_{L,2}$	−192.32
$S_{L,3}$	−132.80
α_0	1.65
α_1	−0.56
α_2	−1.08
α_3	2.97

High-pressure measurements are performed for Jet A-1/air mixture at conditions of $T = 423$ K and $P = 0.1$ – 0.8 MPa for equivalence ratios $\varphi = 0.7$ – 0.8 . As illustrated in Figure 18 laminar flame speeds are plotted with pressure variation using a logarithmic scale. Apart from the experimental data represented

by symbols, the linear fit lines to $S_L = S_{L0} \left(\frac{P}{P_0} \right)^\beta$ ⁴⁴ are also plotted in the same figure. The power exponents β calculated from the experimental results are $\beta_{\varphi=0.7} = -0.235$ and $\beta_{\varphi=0.8} = -0.198$, which demonstrate that, for lean conditions, with increased equivalence ratio value, the exponent power of pressure dependency increases.

3.5. Comparison between Surrogate Kerosene and Jet A-1 Fuels. In order to verify that the Luche surrogate can well simulate the combustion properties of commercial kerosene Jet A-1 in terms of laminar flame speed, in this section, the laminar flame speed of Luche surrogate fuel is compared with commercial jet fuel Jet A-1 for different preheating temperature and pressure conditions. The measure-

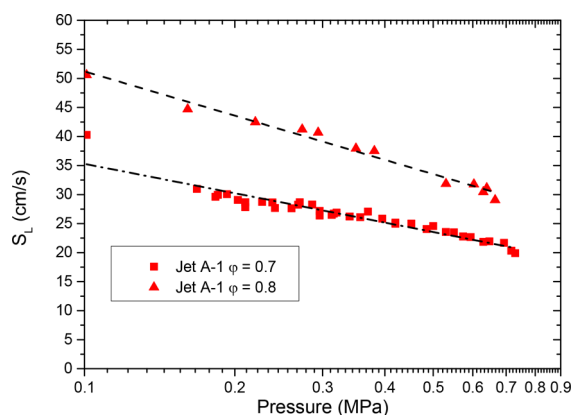


Figure 18. Laminar flame speed of Jet A-1/air mixture at $T = 423$ K, $P = 0.1$ – 0.8 MPa, and $\varphi = 0.7$ and 0.8 (points are our measurements, and dashed lines are linear fits).

ments reported in Figure 19 were performed at $T = 400$ K, $P = 0.1$ MPa, and $\varphi = 0.6$ – 1.3 . The evolution of the laminar flame

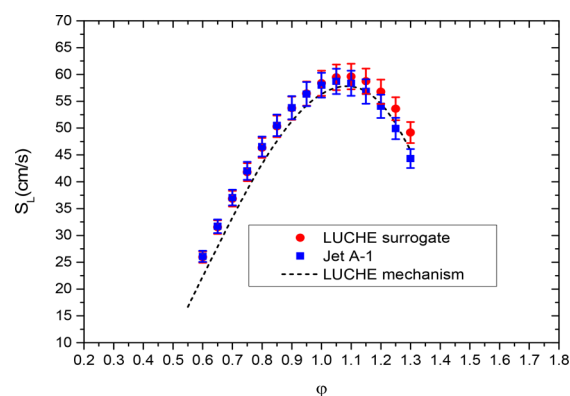


Figure 19. Comparison of the laminar flame speeds of the Luche surrogate fuel and Jet A-1 at conditions of $T = 400$ K, $P = 0.1$ MPa, and $\varphi = 0.6$ – 1.3 .

speed of the Luche surrogate is in good agreement with the flame speeds of Jet A-1 for lean conditions. For rich mixtures, i.e., $\varphi > 1.1$, the Luche surrogate gives faster laminar flame speed values than Jet A-1 commercial fuel. This maximum discrepancy is around 5 cm/s at equivalence ratio condition $\varphi = 1.3$. This tendency is in agreement with that found in the literature that the surrogate fuel normally has a faster flame speed than practical jet fuels.¹⁰ The Luche mechanism simulation results are also in good agreement with measurement results. Tiny discrepancies are however found for fuel-lean mixtures, while a good prediction of measurements is noted for fuel-rich mixtures.

Figure 20 presents the effect of pressure on the laminar flame speeds of both fuels. For all equivalence ratio condition investigated in the present work, it shows that the Luche surrogate and Jet A-1 fuels present certain stunning pressure dependence similarities. However, the Luche mechanism gives slightly lower flame speeds. Meanwhile, it should be noted that the simulation can qualitatively reproduce the pressure dependency on the laminar flame speed.

4. CONCLUSION

The laminar flame speeds of kerosene fuels, including the Luche surrogate, its pure components, and commercial

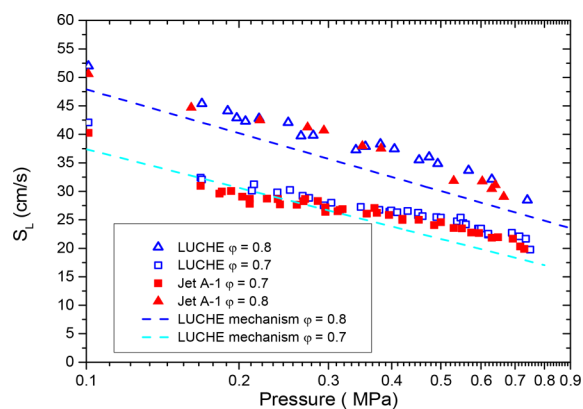


Figure 20. Comparison of the laminar flame speeds of the Luche surrogate and Jet A-1 at conditions of $P = 0.1$ – 0.8 MPa, $T = 423$ K, and $\varphi = 0.7$ – 0.8 .

kerosene Jet A-1, have been studied in the present work. The experiments were first performed for neat components that enter in the commercial kerosene compositions, such as *n*-decane, *n*-propyl benzene, and propyl cyclohexane. Next, measurements of a mixture of these three components (referred to as the Luche surrogate) were conducted. Lastly, efforts have been focused on the measurements of commercial kerosene fuel Jet A-1 over a large range of working conditions including variations of temperature, pressure, and equivalence ratio. It was found that *n*-decane, *n*-propyl benzene, and propyl cyclohexane have quite similar laminar flame speeds. A mixture of these components is able to effectively emulate the combustion property of commercial kerosene fuel (Jet A-1) in terms of laminar flame speed. Meanwhile, a comparison between simulation and experimental results reveals that the Luche skeletal kinetic mechanism slightly underpredicts the laminar flame speeds of the surrogate and practical Jet A-1 fuels for all conditions investigated in the present study.

AUTHOR INFORMATION

Corresponding Author

*E-mail: yi.wu@imech.ac.cn. Phone: +86 132 6018 7692. Fax: +86 10 6256 1284 .

ORCID

Yi Wu: 0000-0002-3255-2702

Notes

The authors declare no competing financial interest.

REFERENCES

- (1) Dooley, S.; Won, S. H.; Jahangirian, S.; Ju, Y.; Dryer, F. L.; Wang, H. The combustion kinetics of a synthetic paraffinic jet aviation fuel and a fundamentally formulated, experimentally validated surrogate fuel. *Combust. Flame* **2012**, *159*, 3014–3020.
- (2) Selle, L.; Lartigue, G.; Poinsot, T.; Koch, R.; Schildmacher, K. U.; Krebs, W. Compressible large eddy simulation of turbulent combustion in complex geometry on unstructured meshes. *Combust. Flame* **2004**, *137*, 489–505.
- (3) Natelson, R. H.; Kurman, M. S.; Cernansky, N. P.; Miller, D. L. Experimental investigation of surrogates for jet and diesel fuels. *Fuel* **2008**, *87*, 2339–2342.
- (4) Cooke, J. A.; Bellucci, M.; Smooke, M. D.; Gomez, A.; Violi, A.; Faravelli, T. Computational and experimental study of JP-8, a surrogate, and its components in counterflow diffusion flames. *Proc. Combust. Inst.* **2005**, *30*, 439–446.
- (5) Honnet, S.; Seshadri, K.; Niemann, U.; Peters, N. A surrogate fuel for kerosene. *Proc. Combust. Inst.* **2009**, *32*, 485–492.

- (6) Luche, J.; Reuillon, M.; Boettner, J.-C.; Cathonnet, M. Reduction of large detailed kinetic mechanism: application to kerosene/air combustion. *Combust. Sci. Technol.* **2004**, *176*, 1935–1963.
- (7) Comandini, A.; Dubois, T.; Chaumeix, N. Laminar flame speeds of n-decane, n-butylbenzene, and n-propylcyclohexane mixtures. *Proc. Combust. Inst.* **2015**, *35*, 671–678.
- (8) Dagaut, P.; El Bakali, A.; Ristori, A. The combustion of kerosene: Experimental results and kinetic modelling using 1- to 3-component surrogate model fuels. *Fuel* **2006**, *85*, 944–956.
- (9) Dooley, S.; Won, S. H.; Chaos, M.; Heyne, J.; Ju, Y.; Dryer, F. L. A jet fuel surrogate formulated by real fuel properties. *Combust. Flame* **2010**, *157*, 2333–2339.
- (10) Dagaut, P.; Cathonnet, M. The ignition, oxidation, and combustion of kerosene: A review of experimental and kinetic modeling. *Prog. Energy Combust. Sci.* **2006**, *32*, 48–92.
- (11) Hui, X.; Das, A. K.; Kumar, K.; Sung, C.-J.; Dooley, S.; Dryer, F. L. Laminar flame speeds and extinction stretch rates of selected aromatic hydrocarbons. *Fuel* **2012**, *97*, 695–702.
- (12) Darcy, D.; Nakamura, H.; Tobin, C. J.; Mehl, M.; Metcalfe, W. K.; Pitz, W. J. A high-pressure rapid compression machine study of n-propylbenzene ignition. *Combust. Flame* **2014**, *161*, 65–74.
- (13) Zhukov, V. P.; Sechenov, V. A.; Starikovskii, A. Y. Autoignition of n-decane at high pressure. *Combust. Flame* **2008**, *153*, 130–136.
- (14) Gauthier, B. M.; Davidson, D. F.; Hanson, R. K. Shock tube determination of ignition delay times in full-blend and surrogate fuel mixtures. *Combust. Flame* **2004**, *139*, 300–311.
- (15) Vasu, S. S.; Davidson, D. F.; Hanson, R. K. Jet fuel ignition delay times: Shock tube experiments over wide conditions and surrogate model predictions. *Combust. Flame* **2008**, *152*, 125–143.
- (16) Agnew, J. T.; Graiff, L. B. The pressure dependence of laminar burning velocity by the spherical bomb method. *Combust. Flame* **1961**, *5*, 209–219.
- (17) Bouvet, N.; Chauveau, C.; Gokalp, I.; Lee, S.-Y.; Santoro, R. J. Characterization of syngas laminar flames using the Bunsen burner configuration. *Int. J. Hydrogen Energy* **2011**, *36*, 992–1005.
- (18) Chong, C. T.; Hochgreb, S. Measurements of laminar flame speeds of acetone/methane/air mixtures. *Combust. Flame* **2011**, *158*, 490–500.
- (19) Hui, X.; Sung, C.-J. Laminar flame speeds of transportation-relevant hydrocarbons and jet fuels at elevated temperatures and pressures. *Fuel* **2013**, *109*, 191–200.
- (20) Denman, B. M.; Munzar, J. D.; Bergthorson, J. M. An Experimental and Numerical Study of the Laminar Flame Speed of Jet Fuel Surrogate Blends. *ASME Turbo Expo 2012: Turbine Technical Conference and Exposition*, Copenhagen, Denmark, June 11, 2012; ASME, 2012; pp 1417–1426.
- (21) Munzar, J. D.; Akih-Kumgeh, B.; Denman, B. M.; Zia, A.; Bergthorson, J. M. An experimental and reduced modeling study of the laminar flame speed of jet fuel surrogate components. *Fuel* **2013**, *113*, 586–597.
- (22) Ji, C.; Egolfopoulos, F. N. Flame propagation of mixtures of air with binary liquid fuel mixtures. *Proc. Combust. Inst.* **2011**, *33*, 955–961.
- (23) Liu, N.; Ji, C.; Egolfopoulos, F. N. Ignition of non-premixed cyclohexane and mono-alkylated cyclohexane flames. *Proc. Combust. Inst.* **2013**, *34*, 873–880.
- (24) Kumar, K.; Sung, C.-J.; Hui, X. Laminar flame speeds and extinction limits of conventional and alternative jet fuels. *Fuel* **2011**, *90*, 1004–1011.
- (25) Holley, A. T.; Dong, Y.; Andac, M. G.; Egolfopoulos, F. N.; Edwards, T. Ignition and extinction of non-premixed flames of single-component liquid hydrocarbons, jet fuels, and their surrogates. *Proc. Combust. Inst.* **2007**, *31*, 1205–1213.
- (26) Won, S. H.; Dooley, S.; Dryer, F. L.; Ju, Y. Kinetic effects of aromatic molecular structures on diffusion flame extinction. *Proc. Combust. Inst.* **2011**, *33*, 1163–1170.
- (27) Won, S. H.; Ju, Y.; Dooley, S.; Dryer, F. Measurement of Extinction Limits and OH Radicals for Trimethylbenzene and n-Propylbenzene Diffusion Flames. *48th AIAA Aerospace Sciences Meeting Including the New Horizons Forum and Aerospace Exposition*, Orlando, FL; American Institute of Aeronautics and Astronautics, 2010.
- (28) Driscoll, J. F. Turbulent premixed combustion: Flamelet structure and its effect on turbulent burning velocities. *Prog. Energy Combust. Sci.* **2008**, *34*, 91–134.
- (29) Ranzi, E.; Frassoldati, A.; Grana, R.; Cuoci, A.; Faravelli, T.; Kelley, A. P. Hierarchical and comparative kinetic modeling of laminar flame speeds of hydrocarbon and oxygenated fuels. *Prog. Energy Combust. Sci.* **2012**, *38*, 468–501.
- (30) Schulz, W. D. Oxidation products of a surrogate JP-8 fuel. *Prepr.-Am. Chem. Soc., Div. Pet. Chem.* **1991**, *37*, 183–392.
- (31) Agosta, A.; Cernansky, N. P.; Miller, D. L.; Faravelli, T.; Ranzi, E. Reference components of jet fuels: kinetic modeling and experimental results. *Exp. Therm. Fluid Sci.* **2004**, *28*, 701–708.
- (32) Violi, A.; Yan, S.; Eddings, E. G.; Sarofim, A. F.; Granata, S.; Faravelli, T. Experimental formulation and kinetic model for JP-8 surrogate mixtures. *Combust. Sci. Technol.* **2002**, *174*, 399–417.
- (33) Montgomery, C.; Cannon, S.; Mawid, M.; Sekar, B. Reduced chemical kinetic mechanisms for JP-8 combustion. *40th AIAA Aerospace Science Meeting & Exhibit*; 2002; 0036.
- (34) Humer, S.; Frassoldati, A.; Granata, S.; Faravelli, T.; Ranzi, E.; Seiser, R. Experimental and kinetic modeling study of combustion of JP-8, its surrogates and reference components in laminar nonpremixed flows. *Proceedings of the Combustion Institute. Proc. Combust. Inst.* **2007**, *31*, 393–400.
- (35) Wood, C. P.; Mcdonell, V. G.; Smith, R. A.; Samuelsen, G. S. Development and application of a surrogate distillate fuel. *J. Propul. Power* **1989**, *5*, 399–405.
- (36) Edwards, T. Surrogate mixtures to represent complex aviation and rocket fuels. *J. Propul. Power* **2001**, *17*, 461.
- (37) Kumar, K.; Sung, C.-J. Laminar flame speeds and extinction limits of preheated n-decane/O₂/N₂ and n-dodecane/O₂/N₂ mixtures. *Combust. Flame* **2007**, *151*, 209–224.
- (38) Vukadinovic, V.; Habisreuther, P.; Zanzalis, N. Influence of pressure and temperature on laminar burning velocity and Markstein number of kerosene Jet A-1: Experimental and numerical study. *Fuel* **2013**, *111*, 401–410.
- (39) Chen, Z. On the accuracy of laminar flame speeds measured from outwardly propagating spherical flames: Methane/air at normal temperature and pressure. *Combust. Flame* **2015**, *162*, 2442–2453.
- (40) Varea, E.; Modica, V.; Renou, B.; Boukhalfa, A. M. Pressure effects on laminar burning velocities and Markstein lengths for Isooctane/Ethanol/Air mixtures. *Proc. Combust. Inst.* **2013**, *34*, 735–744.
- (41) Konnov, A. A.; Riemeijer, R.; de Goey, L. P. H. Adiabatic laminar burning velocities of CH₄ + H₂ + air flames at low pressures. *Fuel* **2010**, *89*, 1392–1396.
- (42) Faith, G. H. A. L.E.; Henderson, H.T. *Heat Sink Capabilities of Jet A Fuel: Heat Transfer and Coking Studies*; Shell Development Co., 1971; NASA CR-72951.
- (43) Wu, Y.; Rossow, B.; Modica, V.; Yu, X.; Wu, L.; Grisch, F. Laminar flame speed of lignocellulosic biomass-derived oxygenates and blends of gasoline/oxygenates. *Fuel* **2017**, *202*, 572–582.
- (44) Wu, Y.; Modica, V.; Rossow, B.; Grisch, F. Effects of pressure and preheating temperature on the laminar flame speed of methane/air and acetone/air mixtures. *Fuel* **2016**, *185*, 577–588.
- (45) Law, C. K.; Ishizuka, S.; Cho, P. On the Opening of Premixed Bunsen Flame Tips. *Combust. Sci. Technol.* **1982**, *28*, 89–96.
- (46) Mizomoto, M.; Asaka, Y.; Ikai, S.; Law, C. K. Effects of preferential diffusion on the burning intensity of curved flames. *Symp. (Int.) Combust., [Proc.]* **1985**, *20*, 1933–1939.
- (47) Vu, T. M.; Cha, M. S.; Lee, B. J.; Chung, S. H. Tip opening of premixed bunsen flames: Extinction with negative stretch and local Karlovitz number. *Combust. Flame* **2015**, *162*, 1614–1621.
- (48) Wang, J.; Wei, Z.; Yu, S.; Jin, W.; Xie, Y.; Zhang, M. Effects of stretch and preferential diffusion on tip opening of laminar premixed Bunsen flames of syngas/air mixtures. *Fuel* **2015**, *148*, 1–8.

- (49) Koch, J. D.; Hanson, R. K. Temperature and excitation wavelength dependencies of 3-pentanone absorption and fluorescence for PLIF applications. *Appl. Phys. B: Lasers Opt.* **2003**, *76*, 319–324.
- (50) Orain, M.; Baranger, P.; Ledier, C.; Apeloig, J.; Grisch, F. Fluorescence spectroscopy of kerosene vapour at high temperatures and pressures: potential for gas turbines measurements. *Appl. Phys. B: Lasers Opt.* **2014**, *116*, 729–745.
- (51) Yu, G.; Law, C. K.; Wu, C. K. Laminar flame speeds of hydrocarbon + air mixtures with hydrogen addition. *Combust. Flame* **1986**, *63*, 339–347.
- (52) Wang, Z. H.; Weng, W. B.; He, Y.; Li, Z. S.; Cen, K. F. Effect of {H₂/CO} ratio and {N₂/CO₂} dilution rate on laminar burning velocity of syngas investigated by direct measurement and simulation. *Fuel* **2015**, *141*, 285–292.
- (53) Gao, X.; Zhang, Y.; Adusumilli, S.; Seitzman, J.; Sun, W.; Ombrello, T. The effect of ozone addition on laminar flame speed. *Combust. Flame* **2015**, *162*, 3914–3924.
- (54) Sun, S.; Meng, S.; Zhao, Y.; Xu, H.; Guo, Y.; Qin, Y. Experimental and theoretical studies of laminar flame speed of CO/H₂ in O₂/H₂O atmosphere. *Int. J. Hydrogen Energy* **2016**, *41*, 3272–3283.
- (55) Natarajan, J.; Lieuwen, T.; Seitzman, J. Laminar flame speeds of H₂/CO mixtures: Effect of {CO₂} dilution, preheat temperature, and pressure. *Combust. Flame* **2007**, *151*, 104–119.
- (56) Mazas, A. N.; Fiorina, B.; Lacoste, D. A.; Schuller, T. Effects of water vapor addition on the laminar burning velocity of oxygen-enriched methane flames. *Combust. Flame* **2011**, *158*, 2428–2440.
- (57) Toulouzan, J. N. L.; Locquet, J. J.; Allano, D.; Savary, P.; Darrigo, R. Abel's inversion of a cylindrical helium plasma. Production of a stigmatic spectrograph using a vidicon detector. *J. Opt.* **1981**, *12*, 369.
- (58) Wang, E. D. H.; Sirjean, B.; Sheen, D. A.; Tango, R.; Violi, A.; Lai, J. Y. W.; Egolfopoulos, F. N.; Davidson, D. F.; Hanson, R. K.; Bowman, C. T.; Law, C. K.; Tsang, W.; Cernansky, N. P.; Miller, D. L.; Lindstedt, R. P. A high-temperature chemical kinetic model of n-alkane (up to n-dodecane), cyclohexane, and methyl-, ethyl-, n-propyl and n-butyl-cyclohexane oxidation at high temperatures. *JetSurF, version 2.0*, Sept 19, 2010; <http://web.stanford.edu/group/haiwanglab/JetSurF/JetSurF2.0/index.html>.
- (59) Munzar, J. D.; Akih-Kumgeh, B.; Denman, B. M.; Zia, A.; Bergthorson, J. M. An experimental and reduced modeling study of the laminar flame speed of jet fuel surrogate components. *Fuel* **2013**, *113*, 586–597.
- (60) Kim, D.; Martz, J.; Violi, A. A surrogate for emulating the physical and chemical properties of conventional jet fuel. *Combust. Flame* **2014**, *161*, 1489–1498.
- (61) Mehl, M.; Herbinet, O.; Dirrenberger, P.; Bounaceur, R.; Glaude, P.-A.; Battin-Leclerc, F. Experimental and modeling study of burning velocities for alkyl aromatic components relevant to diesel fuels. *Proc. Combust. Inst.* **2015**, *35*, 341–348.
- (62) Dubois, T.; Chaumeix, N.; Paillard, C.-E. Experimental and Modeling Study of n-Propylcyclohexane Oxidation under Engine-relevant Conditions. *Energy Fuels* **2009**, *23*, 2453–2466.
- (63) Ji, C.; Dames, E.; Sirjean, B.; Wang, H.; Egolfopoulos, F. N. An experimental and modeling study of the propagation of cyclohexane and mono-alkylated cyclohexane flames. *Proc. Combust. Inst.* **2011**, *33*, 971–978.
- (64) WU, F.; Kelley, P. A.; Law, C. K. Laminar flame speed of cyclohexane and mono-alkylated cyclohexanes at elevated pressures. *Combust. Flame* **2011**, *159*, 1417–1425.
- (65) Metghalchi, M.; Keck, J. C. Burning velocities of mixtures of air with methanol, isooctane, and indolene at high pressure and temperature. *Combust. Flame* **1982**, *48*, 191–210.